

Microscopic study of fusion reactions with a weakly bound nucleus: Effects of deformed haloXiang-Xiang Sun (孙向向)  and Lu Guo (郭璐)**School of Nuclear Science and Technology, University of Chinese Academy of Sciences, Beijing 100049, China
and CAS Key Laboratory of Theoretical Physics, Institute of Theoretical Physics, Chinese Academy of Sciences, Beijing 100190, China*

(Received 30 August 2022; accepted 17 November 2022; published 4 January 2023)

We present a microscopic study on the fusion reactions $^{14,15}\text{C} + ^{232}\text{Th}$ by emphasizing the effect of deformed halo structure on reaction dynamics within the framework of time-dependent density functional theory. The internuclear potentials are obtained by using the density-constraint frozen Hartree-Fock approach and then are adopted to calculate the fusion cross sections of $^{14,15}\text{C} + ^{232}\text{Th}$, taking all the orientations of deformed reactants into account. Our microscopic calculations not only reproduce the enhancement of fusion cross sections at sub-barrier energies without any adjustable parameters, but also reveal the underlying mechanism of this enhancement, which is driven by the deformed halo structure of ^{15}C . More interestingly, by performing particle number projection based on the wave functions from time-dependent Hartree-Fock simulation, we find that the one-neutron transfer probabilities are more sensitive to the orientations of ^{15}C than ^{232}Th , indicating the notable effects of halo structure on the reaction dynamics.

DOI: [10.1103/PhysRevC.107.L011601](https://doi.org/10.1103/PhysRevC.107.L011601)

Introduction. The nuclear halo is one of the exotic nuclear phenomena and is notably characterized by the small nucleon separation energy and the enhancement of matter radius as a result of weakly bound valence nucleons occupying *s*- or *p*-wave orbitals. The nuclear halo phenomenon was first observed in ^{11}Li [1] and later in dozens of nuclei, including ^6He , $^{17,19}\text{B}$, $^{15,19,22}\text{C}$, ^{29}F [2–5]. The formation of the halo and its structure are closely related to many factors including pairing correlations, continuum, deformation effects, shell evolution, and the interplay among them [6–12]. These characteristics of halos can also manifest themselves in the low-energy heavy-ion reaction with halo nuclei as reactants.

Fusion reactions involving halo nuclei have gained lots of special attention during the last several decades [13–18]. Cross sections for several fusion reactions involving halo nuclei have been measured, including $^{11}\text{Li} + ^{209}\text{Bi}$, $^6\text{He} + ^{238}\text{U}$, $^6\text{He} + ^{209}\text{Bi}$, $^{11}\text{Be} + ^{209}\text{Bi}$, $^{15}\text{C} + ^{232}\text{Th}$, and so on (see Refs. [17,18] for recent reviews). Usually, a halo nucleus is regarded as a system consisting of a core plus one (two) weakly bound valence nucleon(s). Such properties lead to complexities in the description of reactions involving halo nuclei and influence the systematics of cross sections. It has been shown that the fusion cross sections of $^{11}\text{Li} + ^{208}\text{Pb}$ at sub-barrier energies are enhanced compared with those of $^7,9\text{Li} + ^{209}\text{Pb}$ [19]. Similar observations are also found in the fusions of $^{11,10}\text{Be} + ^{209}\text{Bi}$ [20], $^4,6\text{He}$ with ^{208}Pb or ^{209}Bi [21,22], and $^{12,13,14,15}\text{C} + ^{232}\text{Th}$ [23]. It should be mentioned that this enhancement is not found in $^6\text{He} + ^{238}\text{U}$ [24], which might be due to the fissility of ^{238}U . Generally speaking, the underlying mechanism of reactions involving weakly

bound nuclei is still not completely understood, and a microscopic study on this issue with no free parameters still has not been achieved.

Theoretically, the fusion cross sections of reactions with weakly bound nuclei can be well described by using the coupled-channels and continuum discretized coupled-channels approaches [15–18]. The adopted internuclear interactions in these two approaches are usually phenomenological ones containing several adjustable parameters, which might influence the predictive power and the capability to reveal the reaction mechanism. To date, the time-dependent density functional theory (TDDFT) starting from the effective nucleon-nucleon interactions has been successfully applied in many aspects of low-energy heavy-ion reactions [25–30] including fusion reactions. One of the advantages of TDDFT is that it can microscopically explore how the structures of reactants affect reaction dynamics [31], and the resulting conclusions are only dependent on the adopted density functionals, in which the parameters are determined by fitting to nuclear bulk properties. As far as we know, the TDDFT has not been used to study fusion reactions with halo nuclei.

Among the reaction systems mentioned above, $^{15}\text{C} + ^{232}\text{Th}$ is of particular interest because ^{15}C has a one-neutron halo structure [2,32] and ^{232}Th is a deformed nucleus [33], and it is significant to explore the effects of these nuclear structures on the reaction mechanism. The calculations in Refs. [23,34] fail to reproduce the data at sub-barrier energies, and recently the influence of the deformation of ^{232}Th on fusion cross sections were studied, describing the halo structure ^{15}C phenomenologically, and the adopted internuclear interactions were obtained by using a double-folding approach [35]. It has been shown that the halo in ^{15}C is not totally dominated by the *s* wave [2], and calculations with density functional theories have shown that the ground state of ^{15}C has a prolate

*luguo@ucas.ac.cn

shape [36,37]. In this work, aiming at describing the nuclear structure properties and reaction dynamics self-consistently, we study the ground state properties, investigate the fusions involving a one-neutron halo nucleus, and reveal the influence of halo structure of ^{15}C on reaction mechanisms in a uniformed TDDFT framework.

Theoretical framework. In the time-dependent Hartree-Fock (TDHF) theory, the Hamiltonian of the reaction system is a functional of various densities and the dynamic process is described by the time-dependent single Slater determinant $|\Psi\rangle$ composed of the single-particle wave function $\psi_i(\mathbf{r}, t)$ governed by the TDHF equations

$$i\hbar \frac{\partial}{\partial t} \psi_i(\mathbf{r}, t) = h\psi_i(\mathbf{r}, t) \quad (i = 1, \dots, A), \quad (1)$$

where h is the single-particle Hamiltonian and A is the number of single-particle states. These non-linear equations are solved on a three-dimensional Cartesian grid without any symmetry restrictions [38]. The fusion cross section for above-barrier energies can be estimated by the sharp cutoff approximation over the impact parameter. The lack of quantum tunneling of the many-body wave function means that the TDHF theory cannot be directly used to study sub-barrier fusion reactions. Most of the theoretical approaches for fusion cross section start with the internuclear potentials. Based on the densities from static HF or TDHF calculations one can obtain the microscopic internuclear potentials, which only rely on the adopted density functional and do not contain any adjustable parameters, by using the frozen HF [39], density constrained (DC) TDHF [40], and DC frozen HF (DC-FHF) methods [41]. The potentials from DC-TDHF have been applied to many systems, and good agreements with experimental fusion cross sections have been achieved [30,42–49], but the potentials from DC-TDHF, which contain the effects from dynamic excitations and are dependent on incident energies, cannot be directly used in coupled-channels analyses [41]. The potential from FHF does not consider the effects of the Pauli principle [41,50], which are included in DC-FHF and DC-TDHF by allowing the rearrangement of single-particle states in the variation procedure. We also note that the DC-FHF method has not been applied to deformed systems. In this work, to investigate the influence of the deformed halo structure of ^{15}C on the fusion cross sections, we use the orientation-average formulas with the penetration probabilities calculated by CCFULL under the internuclear potentials from the DC-FHF method.

For fusion reaction between deformed nuclei, in principle one should consider the orientation angles along both the direction perpendicular to the reaction plane and the collision direction. This means a total of four orientation angles to be averaged for the deformed target and projectile. In most theoretical calculations of fusion cross sections [35,51–53], usually the orientation angles along the direction perpendicular to the reaction plane are averaged and the other angles are treated with equal weights. Additionally, if here we consider the internuclear potentials for all the possible orientations with four angles, we need to calculate several thousand potentials using DC-FHF, which needs nearly 10^6 CPU hours only for calculating the internuclear potentials, and costs too much.

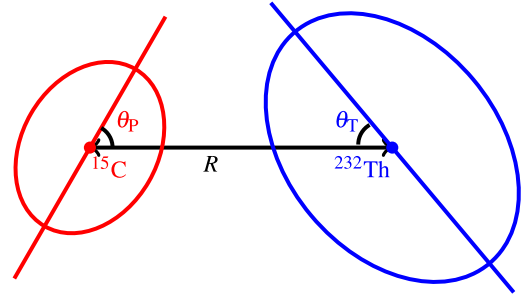


FIG. 1. Relative position of deformed projectile and target. θ_p (θ_T) labels the angle between the symmetry axis of the deformed projectile (target) and the collision axis (denoted by the black line).

Therefore, in this work we consider the orientation angles along the the direction perpendicular to the reaction plane.

To obtain the potential at each orientation with DC-FHF method, the HF calculations are performed constraining the total proton p and neutron n densities to be the same as those of the ground state,

$$\delta \left\langle H - \int d^3r \sum_{q=p,n} \lambda_q(\mathbf{r}) [\rho_{P,q}(\mathbf{r}; \theta_p) + \rho_{T,q}(\mathbf{r} - \mathbf{R}; \theta_T)] \right\rangle = 0, \quad (2)$$

where $\rho_p(\theta_p)$ and $\rho_T(\theta_T)$ are densities of the projectile and target for a given orientation labeled by (θ_p, θ_T) , which can be achieved by performing Eulerian rotations of Slater determinants in a three-dimensional Cartesian geometry [54]. $\theta_p(\theta_T)$ denotes the angles between the principle axis of projectile (target) and the collision direction, as shown in Fig. 1. This variation procedure results in a unique Slater determinant $\Phi(\mathbf{R})$. The internuclear potential is given by

$$V_{\text{DC-FHF}}(R; \theta_p, \theta_T) = \langle \Phi(\mathbf{R}) | H | \Phi(\mathbf{R}) \rangle (\theta_p, \theta_T) - E_p - E_T, \quad (3)$$

where E_p and E_T are binding energies of projectile and target, respectively.

Subsequently, to calculate the penetration probabilities $T_J(E_{c.m.})$ corresponding to orbital angular momentum J , i.e., different impact parameters, we solve the Schrödinger equation with the potential from the DC-FHF method,

$$\left[\frac{-\hbar^2}{2\mu} \frac{d^2}{dR^2} + \frac{J(J+1)\hbar^2}{2\mu R^2} + V_{\text{DC-FHF}}(R) - E_{c.m.} \right] \psi(R) = 0, \quad (4)$$

by using the incoming wave boundary condition method [55]. The capture cross sections at energies below and above the barrier for each orientation (θ_T, θ_p) are then calculated as

$$\sigma_{\text{cap}}(E_{c.m.}, \theta_T, \theta_p) = \frac{\pi}{k^2} \sum_J (2J+1) T_J(E_{c.m.}), \quad (5)$$

where $k = \sqrt{2\mu E_{c.m.}/\hbar^2}$ with μ being the reduced mass in the entrance channel, and the summation is over all possible angular momenta. $T_J(E_{c.m.})$ is the penetration probability for given incident energy $E_{c.m.}$ and angular momentum J . For fusion reactions with deformed systems, the cross section can

be calculated by using the orientation average formula [51]

$$\sigma_{\text{fus}}(E_{\text{c.m.}}) = \int_0^1 d \cos(\theta_{\text{p}}) \int_0^1 d \cos(\theta_{\text{T}}) \sigma(E_{\text{c.m.}}, \theta_{\text{p}}, \theta_{\text{T}}). \quad (6)$$

To calculate the nucleon transfer probabilities the particle number projection technique (PNPT) [56] is performed on the final wave functions of TDHF evolution. The probability $P_V(N)$ of N particle in the subspace V reads

$$P_V(N) = \frac{1}{2\pi} \int_0^{2\pi} d\vartheta e^{-iN\vartheta} \langle \Psi | e^{-i\hat{N}_V \vartheta} | \Psi \rangle, \quad (7)$$

where \hat{N}_V is the particle number operator in the subspace V and ϑ is the gauge angle. More details can be found in Refs. [57,58].

Results and discussions. Experimentally it has been shown that ^{14}C is a magic nucleus with the magic number $N = 8$, and the halo of ^{15}C is attributed to the valence neutron partially occupying the s -wave orbital [32]. By using the self-consistent mean-field calculations, it has been shown that the ground state of ^{15}C has a prolate shape [36,37] and the valence neutron is unpaired, thus pairing correlations do not influence its ground-state properties. In this work, the ground state of ^{15}C is calculated exactly with the contributions from time-even and time-odd terms (see Refs. [59–62] for details). In our static HF calculations with the three-dimensional grid $28 \times 28 \times 28 \text{ fm}^3$ by using density functionals SLy5 [63], SLy4d [64], UNEDF0 [65], and UNEDF1 [66], one-neutron separation energies with SLy5 and SLy4d are about 1.5 MeV, which is close to the measurement 1.28 MeV [67]. One-neutron separation energies with UNEDF0 and UNEDF1 are slightly larger than 2 MeV and overestimate the experimental data. The quadrupole deformation parameters β_2 from these density functionals are all close to 0.15. The matter radii R_m without including center-of-mass motion are about 2.65 and 2.77 fm for ^{14}C and ^{15}C , which are larger than the experimental values 2.33(7) and 2.54(4) fm [68]. It should be noted when considering the correction from center-of-mass motion that the calculations still overestimate the matter radii but the discrepancies between calculations and experiments become smaller. The center-of-mass motion is not taken into account because it is usually not considered in TDHF calculations [25–29]. Recently, the density functional SLy5 has been adopted in many investigations [40,49,60,62,69–72], and we use this interaction in following calculations. In Fig. 2, we show the two-dimensional total density distributions of ^{14}C and ^{15}C . It is clear that the spatial extension of ^{15}C is obviously wider than that of ^{14}C . The ground states of ^{14}C and ^{15}C have spherical and prolate shapes, respectively. The amplitude of the s -wave component in the valence neutron orbital of ^{15}C , which can be approximately calculated as the overlap between the single-particle wave functions in the ground state and the wave function of $2s_{1/2}$ in the spherical limit, is about 20%, which is smaller than the values given in Ref. [2]. Therefore, ^{15}C has a deformed halo caused by the s wave in the calculations with SLy5, which is similar to the conclusion given in Ref. [37]. As for ^{232}Th , the static HF calculation shows an axially deformed ground state with

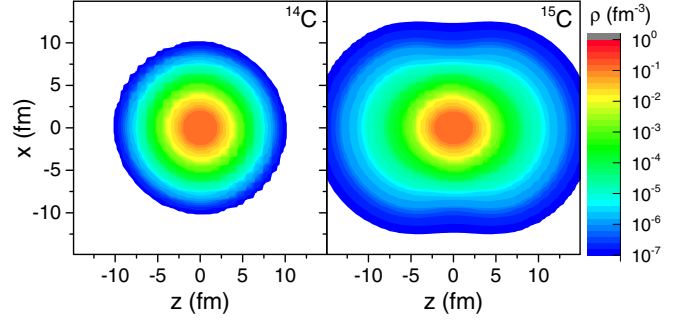


FIG. 2. Two-dimensional density distribution for the ground states of ^{14}C and ^{15}C in the static HF calculations with the density functional SLy5. The z axis is the symmetry axis.

$R_m = 5.86 \text{ fm}$ and $\beta_2 = 0.25$, which is very consistent with the experimental data [33]. Other high-order deformations are self-consistently included in our calculations for ground states and internuclear potentials.

To study the internuclear potentials for deformed system, we have implemented the DC-FHF method [41] based on the modified version of the SKY3D code [38], which has been used in Refs. [49,58–62,69–74]. After getting the ground state densities, the DC-FHF calculations are performed in a three-dimensional grid with size $42 \times 28 \times 28 \text{ fm}^3$ and the grid spacing in each direction is taken to be 1 fm, which have been checked for achieving good numerical accuracy for all the cases studied here. For calculating the total fusion cross sections, we use the Gaussian-quadrature to treat the integral in Eq. (6). Since the ground states of reactants ^{15}C and ^{232}Th are axially deformed, the number of the mesh points for θ_{p} and θ_{T} in the interval $[0^\circ, 90^\circ]$ are all taken to be 7, which means that we totally get 49 internuclear potentials to calculate fusion cross sections. To study the deformation effects of ^{15}C we also calculate the potentials with $\theta_{\text{p}} = 0^\circ$ (tip) and $\theta_{\text{p}} = 90^\circ$ (side), i.e., 14 potentials are obtained additionally. Since ^{14}C has a spherical ground state 7 potentials are calculated for $^{14}\text{C} + ^{232}\text{Th}$. Therefore in the present work, we totally calculated 70 internuclear potentials and the computation cost of each potential is about hundreds of CPU hours, which needs much computational cost.

In Fig. 3, the internuclear potentials for $^{14,15}\text{C} + ^{232}\text{Th}$ for selected orientations are displayed. For $^{14}\text{C} + ^{232}\text{Th}$, since ^{14}C is spherical, the internuclear potentials are dependent on the orientations of the target ^{232}Th . It is clear that the Coulomb barrier of side orientation is higher than that of tip orientation. By comparing the potentials constructed from double folding method given in Ref. [35] with those from DC-FHF, for $^{14}\text{C} + ^{232}\text{Th}$ the barriers in the latter case are slightly higher than the former about 1.5 MeV. In Fig. 3, we also show the internuclear potentials for $^{15}\text{C} + ^{232}\text{Th}$ for four selected orientations. The barrier heights of $^{15}\text{C} + ^{232}\text{Th}$ are always lower than those of $^{14}\text{C} + ^{232}\text{Th}$ for a given θ_{T} . For a fixed orientation of target, the orientation of ^{15}C also influence the barriers and the barrier height between tip and side orientations of ^{15}C differs about 2 MeV. Lowering of the Coulomb barrier leads to an increase of fusion cross sections such that

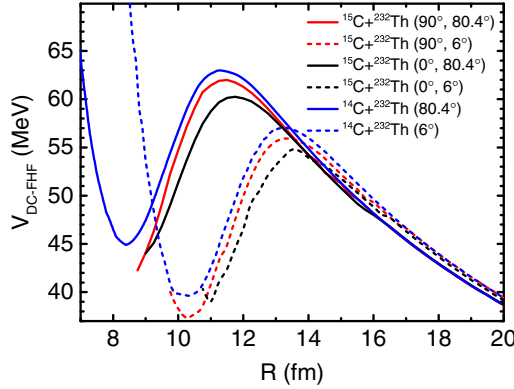


FIG. 3. Internuclear potentials for $^{14,15}\text{C} + ^{232}\text{Th}$ by using the DC-FHF method with SLy5 density functional. For $^{15}\text{C} + ^{232}\text{Th}$ the selected potentials are labeled as the orientations of ^{15}C and ^{232}Th : θ_p and θ_T . 6° and 80.4° are the first and last nodes for seven-point Gaussian quadrature. For $^{14}\text{C} + ^{232}\text{Th}$, ^{14}C has a spherical ground state and the selected potentials are labeled as the orientation of ^{232}Th : θ_T .

we can deduce that the deformed halo structure of ^{15}C also influences the fusion cross sections.

After obtaining the internuclear potentials for different orientations, one can calculate the total fusion cross sections by using Eq. (6). The calculated results and the comparison with experimental data [23] are shown in Fig. 4. The fusion cross sections using average orientations of target and projectile are shown by red and black solid lines for $^{14}\text{C} + ^{232}\text{Th}$ and $^{15}\text{C} + ^{232}\text{Th}$, respectively. It is clear that our microscopic calculations without free parameters can well reproduce the measured fusion cross sections for two reaction systems, and the enhancement of fusion cross section at sub-barrier energies is found, i.e., cross sections of ^{15}C are larger than those of ^{14}C below barrier, indicating the predictive power of our mi-

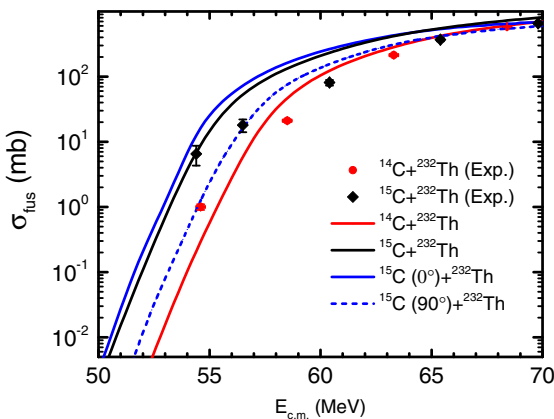


FIG. 4. The comparison between calculated fusion cross sections and experimental ones for $^{14,15}\text{C} + ^{232}\text{Th}$. Experimental data of $^{14}\text{C} + ^{232}\text{Th}$ and $^{15}\text{C} + ^{232}\text{Th}$ are taken from Ref. [23] and labeled by red solid circles and black solid diamonds, respectively. Calculated fusion cross sections for $^{14}\text{C} + ^{232}\text{Th}$ and $^{15}\text{C} + ^{232}\text{Th}$ are shown by red and black lines. The blue solid and dashed lines represent the fusion cross sections with tip and side orientations of ^{15}C , respectively.

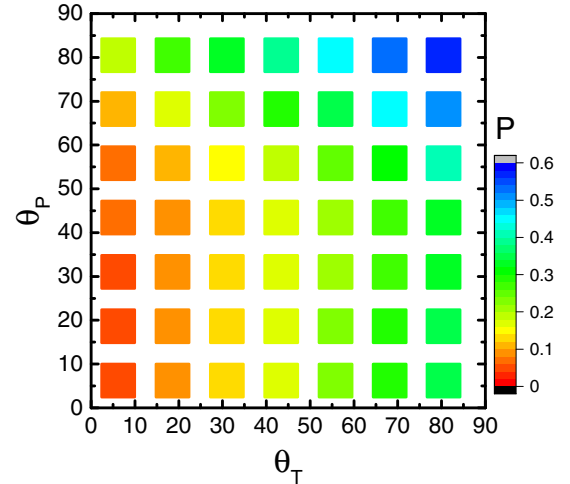


FIG. 5. Calculated one-neutron transfer probability of the fusion reaction $^{15}\text{C} + ^{232}\text{Th}$ by using TDHF with the particle number projection technique. The incident energies for all orientations are taken to be 54 MeV.

croscopic approach. Additionally, we also present the fusion cross sections for $^{15}\text{C} + ^{232}\text{Th}$ with ^{15}C having side and tip orientations while all the orientations of ^{232}Th are considered. At sub-barrier region fusion cross sections of both side and tip orientations of ^{15}C are all larger than those of $^{14}\text{C} + ^{232}\text{Th}$. This is because ^{15}C has a one-neutron halo structure and both the charge and matter radii of ^{15}C are obviously larger than those of ^{14}C [68] such that the Coulomb barrier is lower and fusion cross sections are increased further. The calculated fusion cross sections for the sub-barrier region with $\theta_p = 90^\circ$ are smaller than the experimental data while those for $\theta_p = 0^\circ$ are larger than data. After averaging the orientations of ^{15}C , a nice agreement between measurements and calculations in the sub-barrier region is achieved. This shows that orientation of ^{15}C plays an important role in the description of sub-barrier fusions.

To study neutron transfer, we perform the TDHF calculations with the PNPT [56–58,71] to calculate the probability of the channel $^{14}\text{C} + ^{233}\text{Th}$. In realistic calculations, after obtaining the time evolution of $^{15}\text{C} + ^{232}\text{Th}$ for 49 orientations with the incident energy of 54 MeV, which is below all the Coulomb barriers for 49 calculated internuclear potentials, the PNPT is carried out for the light fragment to get the transfer probabilities. The obtained one-neutron transfer channel probabilities are shown in Fig. 5, and the probabilities for other channels are very small and are not given. It is clear that the probabilities of the one-neutron transfer channel strongly rely on the orientations. The orientations close to side-to-side have larger transfer probabilities while those close to tip-to-tip become smaller. The dependence of transfer probabilities on the orientation of ^{15}C is much stronger than ^{232}Th , indicating the important role of one-neutron halo structure.

From above discussions, our microscopic study has revealed that the enhancement of sub-barrier fusion cross sections for ^{15}C is related to the deformed one-neutron halo structure. However, there exist discrepancies between calculations and experiments. For ^{14}C , a tightly bound nucleus, the

breakup channel should have no influence and the difference between calculations and experimental data might originate from the adopted density functional. As for $^{15}\text{C} + ^{232}\text{Th}$, the discrepancies might be related to the absence of breakup effects in our microscopic calculations of fusion cross sections. But we can discuss the influence of one-neutron transfer on cross section from a simple picture. In our calculations the fusion cross sections for $^{14}\text{C} + ^{232}\text{Th}$ in the above-barrier region are generally well reproduced and are smaller than those of $^{15}\text{C} + ^{232}\text{Th}$. The internuclear potentials of $^{14}\text{C} + ^{233}\text{Th}$ should be almost the same to those of $^{14}\text{C} + ^{232}\text{Th}$, leading to the cross sections of these two systems being almost equal to each other. Thus one can assume that the total fusion cross sections of $^{15}\text{C} + ^{232}\text{Th}$ can be approximated as the mixing of two channels: $^{15}\text{C} + ^{232}\text{Th}$ and $^{14}\text{C} + ^{233}\text{Th}$. Thus the above-barrier cross sections is lowered after considering the one-neutron transfer channel. However, a microscopic treatment is still a very important open question in fusion reactions and it is very difficult to self-consistently treat it. It is meaningful to develop a strategy to examine how the transfer channels influence fusion cross sections based on the framework of TDHF and DCFHF, but this is beyond the scope of the present investigation.

Summary. We have presented a microscopic study of fusion reaction involving a one-neutron halo nucleus based on the self-consistent descriptions of nuclear structure properties of reactants and reaction dynamics. The static HF calculation shows that the ground state of ^{15}C has a deformed halo structure, and so the effect of a deformed halo on fusion of $^{15}\text{C} + ^{232}\text{Th}$ has been studied. By performing coupled-channels calculations for $^{14,15}\text{C} + ^{232}\text{Th}$ with the internuclear potentials obtained from DC-FHF, the enhance-

ment of sub-barrier fusion cross sections is reproduced and our study demonstrates that this phenomenon is attributed to the one-neutron halo structure of ^{15}C . The one-neutron transfer probabilities are strongly dependent on deformation orientations and more sensitive to the orientations of ^{15}C than ^{232}Th , indicating the importance of the deformed halo in ^{15}C . The method presented in this work can also be extended to other fusions involving weakly bound nuclei, thus providing a microscopic description which only depends on the adopted effective nucleon-nucleon interaction. This is helpful and meaningful to reveal the relationship between exotic nuclear structure and the reaction mechanism. More comprehensive studies will explore the dependence of fusion reactions on the adopted density functional, since it directly determines the structures of reactants, and will incorporate the contribution from the one-neutron transfer channel to the fusion cross section based on the present microscopic approaches.

Acknowledgments. We thank Liang Li for the discussions on performing Eulerian rotations, Yun Huang for calculating the wave functions of ^{15}C in the spherical limit, Zhen-Ji Wu for the discussions on PNPT, and also Bing Wang and Shan-Gui Zhou for helpful discussions and suggestions. This work has been supported by the Strategic Priority Research Program of the Chinese Academy of Sciences (Grant No. XDB34010000), the National Natural Science Foundation of China (Grant No. 11975237), the Fundamental Research Funds for the Central Universities (Grant No. E2E46302), and the China Postdoctoral Science Foundation (Grant No. 2022M713106). The results described in this paper were obtained using the High-Performance Computing Cluster of the Institute of Theoretical Physics, Chinese Academy of Sciences.

-
- [1] I. Tanihata, H. Hamagaki, O. Hashimoto, Y. Shida, N. Yoshikawa, K. Sugimoto, O. Yamakawa, T. Kobayashi, and N. Takahashi, *Phys. Rev. Lett.* **55**, 2676 (1985).
- [2] I. Tanihata, H. Savajols, and R. Kanungo, *Prog. Part. Nucl. Phys.* **68**, 215 (2013).
- [3] Z. H. Yang, Y. Kubota, A. Corsi, K. Yoshida, X.-X. Sun, J. G. Li, M. Kimura, N. Michel, K. Ogata, C. X. Yuan, Q. Yuan, G. Authalet, H. Baba, C. Caesar, D. Calvet, A. Delbart, M. Dozono, J. Feng, F. Flavigny, J.-M. Gheller *et al.*, *Phys. Rev. Lett.* **126**, 082501 (2021).
- [4] K. J. Cook, T. Nakamura, Y. Kondo, K. Hagino, K. Ogata, A. T. Saito, N. L. Achouri, T. Aumann, H. Baba, F. Delaunay, Q. Deshayes, P. Doornenbal, N. Fukuda, J. Gibelin, J. W. Hwang, N. Inabe, T. Isobe, D. Kameda, D. Kanno, S. Kim *et al.*, *Phys. Rev. Lett.* **124**, 212503 (2020).
- [5] S. Bagchi, R. Kanungo, Y. K. Tanaka, H. Geissel, P. Doornenbal, W. Horiuchi, G. Hagen, T. Suzuki, N. Tsunoda, D. S. Ahn, H. Baba, K. Behr, F. Browne, S. Chen, M. L. Cortés, A. Estradé, N. Fukuda, M. Holl, K. Itahashi, N. Iwasa *et al.*, *Phys. Rev. Lett.* **124**, 222504 (2020).
- [6] P. G. Hansen and B. Jonson, *Europhys. Lett.* **4**, 409 (1987).
- [7] J. Meng, H. Toki, S. G. Zhou, S. Q. Zhang, W. H. Long, and L. S. Geng, *Prog. Part. Nucl. Phys.* **57**, 470 (2006).
- [8] A. S. Jensen, K. Riisager, D. V. Fedorov, and E. Garrido, *Rev. Mod. Phys.* **76**, 215 (2004).
- [9] T. Frederico, A. Delfino, L. Tomio, and M. Yamashita, *Prog. Part. Nucl. Phys.* **67**, 939 (2012).
- [10] J. Meng and S.-G. Zhou, *J. Phys. G: Nucl. Part. Phys.* **42**, 093101 (2015).
- [11] X.-X. Sun, J. Zhao, and S.-G. Zhou, *Phys. Lett. B* **785**, 530 (2018).
- [12] X.-X. Sun and S.-G. Zhou, *Sci. Bull.* **66**, 2072 (2021).
- [13] C. H. Dasso and A. Vitturi, *Phys. Rev. C* **50**, R12 (1994).
- [14] L. Canto, P. Gomes, R. Donangelo, and M. Hussein, *Phys. Rep.* **424**, 1 (2006).
- [15] L. Canto, P. Gomes, R. Donangelo, J. Lubian, and M. Hussein, *Phys. Rep.* **596**, 1 (2015).
- [16] B. B. Back, H. Esbensen, C. L. Jiang, and K. E. Rehm, *Rev. Mod. Phys.* **86**, 317 (2014).
- [17] L. F. Canto, V. Guimarães, J. Lubián, and M. S. Hussein, *Eur. Phys. J. A* **56**, 281 (2020).
- [18] K. Hagino, K. Ogata, and A. M. Moro, *Prog. Part. Nucl. Phys.* **125**, 103951 (2022).
- [19] A. M. Vinodkumar, W. Loveland, R. Yanez, M. Leonard, L. Yao, P. Bricault, M. Dombisky, P. Kunz, J. Lassen, A. C. Morton, D. Ottewell, D. Preddy, and M. Trinczek, *Phys. Rev. C* **87**, 044603 (2013).

- [20] C. Signorini, A. Yoshida, Y. Watanabe, D. Pierroutsakou, L. Stroe, T. Fukuda, M. Mazzocco, N. Fukuda, Y. Mizoi, M. Ishihara, H. Sakurai, A. Diaz-Torres, and K. Hagino, *Nucl. Phys. A* **735**, 329 (2004).
- [21] J. J. Kolata, V. Guimarães, D. Peterson, P. Santi, R. White-Stevens, P. A. DeYoung, G. F. Peaslee, B. Hughey, B. Atalla, M. Kern, P. L. Jolivet, J. A. Zimmerman, M. Y. Lee, F. D. Becchetti, E. F. Aguilera, E. Martinez-Quiroz, and J. D. Hinnefeld, *Phys. Rev. Lett.* **81**, 4580 (1998).
- [22] S. M. Lukanov, Y. E. Penionzhkevich, R. A. Astabatian, N. A. Demekhina, Z. Dlouhy, M. P. Ivanov, R. Kalpakchieva, A. A. Kulko, E. R. Markarian, V. A. Maslov, R. V. Revenko, N. K. Skobelev, V. I. Smirnov, Y. G. Sobolev, W. Trazska, and S. V. Khlebnikov, *Phys. Lett. B* **670**, 321 (2009).
- [23] M. Alcorta, K. E. Rehm, B. B. Back, S. Bedoor, P. F. Bertone, C. M. Deibel, B. DiGiiovine, H. Esbensen, J. P. Greene, C. R. Hoffman, C. L. Jiang, J. C. Lighthall, S. T. Marley, R. C. Pardo, M. Paul, A. M. Rogers, C. Ugalde, and A. H. Wuosmaa, *Phys. Rev. Lett.* **106**, 172701 (2011).
- [24] R. Raabe, J. L. Sida, J. L. Charvet, N. Alamanos, C. Angulo, J. M. Casandjian, S. Courtin, A. Drouart, D. J. C. Durand, P. Figuera, A. Gillibert, S. Heinrich, C. Jouanne, V. Lapoux, A. Lepine-Szily, A. Musumarra, L. Nalpas, D. Pierroutsakou, M. Romoli, K. Rusek, and *et al.*, *Nature (London)* **431**, 823 (2004).
- [25] C. Simenel, *Eur. Phys. J. A* **48**, 152 (2012).
- [26] C. Simenel and A. Umar, *Prog. Part. Nucl. Phys.* **103**, 19 (2018).
- [27] P. Stevenson and M. Barton, *Prog. Part. Nucl. Phys.* **104**, 142 (2019).
- [28] A. S. Umar and V. E. Oberacker, *Nucl. Phys. A* **944**, 238 (2015).
- [29] K. Sekizawa, *Front. Phys.* **7**, 20 (2019).
- [30] X.-X. Sun and L. Guo, *Commun. Theor. Phys.* **74**, 097302 (2022).
- [31] C. Simenel, M. Dasgupta, D. J. Hinde, and E. Williams, *Phys. Rev. C* **88**, 064604 (2013).
- [32] D. Q. Fang, T. Yamaguchi, T. Zheng, A. Ozawa, M. Chiba, R. Kanungo, T. Kato, K. Morimoto, T. Ohnishi, T. Suda, Y. Yamaguchi, A. Yoshida, K. Yoshida, and I. Tanihata, *Phys. Rev. C* **69**, 034613 (2004).
- [33] B. Pritychenko, M. Birch, B. Singh, and M. Horoi, *At. Data Nucl. Data Tables* **107**, 1 (2016).
- [34] V. V. Sargsyan, G. G. Adamian, N. V. Antonenko, W. Scheid, and H. Q. Zhang, *Phys. Rev. C* **86**, 014602 (2012).
- [35] K.-S. Choi, K. S. Kim, M.-K. Cheoun, W. Y. So, and K. Hagino, *Phys. Rev. C* **103**, 034611 (2021).
- [36] H. Sagawa, X. R. Zhou, X. Z. Zhang, and T. Suzuki, *Phys. Rev. C* **70**, 054316 (2004).
- [37] X.-X. Sun, J. Zhao, and S.-G. Zhou, *Nucl. Phys. A* **1003**, 122011 (2020).
- [38] J. Maruhn, P.-G. Reinhard, P. Stevenson, and A. Umar, *Comput. Phys. Commun.* **185**, 2195 (2014).
- [39] L. Guo and T. Nakatsukasa, *EPJ Web Conf.* **38**, 09003 (2012).
- [40] A. S. Umar and V. E. Oberacker, *Phys. Rev. C* **74**, 021601(R) (2006).
- [41] C. Simenel, A. S. Umar, K. Godbey, M. Dasgupta, and D. J. Hinde, *Phys. Rev. C* **95**, 031601(R) (2017).
- [42] A. S. Umar and V. E. Oberacker, *Phys. Rev. C* **77**, 064605 (2008).
- [43] A. S. Umar, V. E. Oberacker, J. A. Maruhn, and P. G. Reinhard, *Phys. Rev. C* **80**, 041601(R) (2009).
- [44] V. E. Oberacker, A. S. Umar, J. A. Maruhn, and P.-G. Reinhard, *Phys. Rev. C* **82**, 034603 (2010).
- [45] R. Keser, A. S. Umar, and V. E. Oberacker, *Phys. Rev. C* **85**, 044606 (2012).
- [46] C. Simenel, R. Keser, A. S. Umar, and V. E. Oberacker, *Phys. Rev. C* **88**, 024617 (2013).
- [47] V. E. Oberacker and A. S. Umar, *Phys. Rev. C* **87**, 034611 (2013).
- [48] A. S. Umar, C. Simenel, and V. E. Oberacker, *Phys. Rev. C* **89**, 034611 (2014).
- [49] K. Godbey, L. Guo, and A. S. Umar, *Phys. Rev. C* **100**, 054612 (2019).
- [50] A. S. Umar, C. Simenel, and K. Godbey, *Phys. Rev. C* **104**, 034619 (2021).
- [51] K. Hagino and N. Takigawa, *Prog. Theor. Phys.* **128**, 1061 (2012).
- [52] B. Wang, K. Wen, W.-J. Zhao, E.-G. Zhao, and S.-G. Zhou, *At. Data Nucl. Data Tables* **114**, 281 (2017).
- [53] V. Sargsyan, S. Grigoryev, G. Adamian, and N. Antonenko, *Comput. Phys. Commun.* **233**, 145 (2018).
- [54] D. A. Pigg, A. S. Umar, and V. E. Oberacker, *Comput. Phys. Commun.* **185**, 1410 (2014).
- [55] K. Hagino, N. Rowley, and A. T. Kruppa, *Comput. Phys. Commun.* **123**, 143 (1999).
- [56] C. Simenel, *Phys. Rev. Lett.* **105**, 192701 (2010).
- [57] K. Sekizawa and K. Yabana, *Phys. Rev. C* **88**, 014614 (2013).
- [58] Z. Wu and L. Guo, *Phys. Rev. C* **100**, 014612 (2019).
- [59] G.-F. Dai, L. Guo, E.-G. Zhao, and S.-G. Zhou, *Phys. Rev. C* **90**, 044609 (2014).
- [60] L. Guo, C. Simenel, L. Shi, and C. Yu, *Phys. Lett. B* **782**, 401 (2018).
- [61] L. Guo, C. Shen, C. Yu, and Z. Wu, *Phys. Rev. C* **98**, 064609 (2018).
- [62] L. Guo, K. Godbey, and A. S. Umar, *Phys. Rev. C* **98**, 064607 (2018).
- [63] E. Chabanat, P. Bonche, P. Haensel, J. Meyer, and R. Schaeffer, *Nucl. Phys. A* **635**, 231 (1998).
- [64] K.-H. Kim, T. Otsuka, and P. Bonche, *J. Phys. G: Nucl. Part. Phys.* **23**, 1267 (1997).
- [65] M. Kortelainen, T. Lesinski, J. Moré, W. Nazarewicz, J. Sarich, N. Schunck, M. V. Stoitsov, and S. Wild, *Phys. Rev. C* **82**, 024313 (2010).
- [66] M. Kortelainen, J. McDonnell, W. Nazarewicz, P.-G. Reinhard, J. Sarich, N. Schunck, M. V. Stoitsov, and S. M. Wild, *Phys. Rev. C* **85**, 024304 (2012).
- [67] M. Wang, W. Huang, F. Kondev, G. Audi, and S. Naimi, *Chin. Phys. C* **45**, 030003 (2021).
- [68] R. Kanungo, W. Horiuchi, G. Hagen, G. R. Jansen, P. Navratil, F. Ameil, J. Atkinson, Y. Ayyad, D. Cortina-Gil, I. Dillmann, A. Estradé, A. Evdokimov, F. Farinon, H. Geissel, G. Guastalla, R. Janik, M. Kimura, R. Knöbel, J. Kurcewicz, Y. A. Litvinov *et al.*, *Phys. Rev. Lett.* **117**, 102501 (2016).
- [69] X.-X. Sun, L. Guo, and A. S. Umar, *Phys. Rev. C* **105**, 034601 (2022).
- [70] X.-X. Sun and L. Guo, *Phys. Rev. C* **105**, 054610 (2022).
- [71] Z. Wu, L. Guo, Z. Liu, and G. Peng, *Phys. Lett. B* **825**, 136886 (2022).
- [72] L. Li, L. Guo, K. Godbey, and A. S. Umar, *Phys. Lett. B* **833**, 137349 (2022).
- [73] X. Li, Z. Wu, and L. Guo, *Sci. China: Phys. Mech. Astron* **62**, 122011 (2019).
- [74] Z. Wu and L. Guo, *Sci. China Phys. Mech. Astron.* **63**, 242021 (2020).